Volume 3
Number 2
February 2024
Pages 157–328

Sensors & Diagnostics

rsc.li/sensors

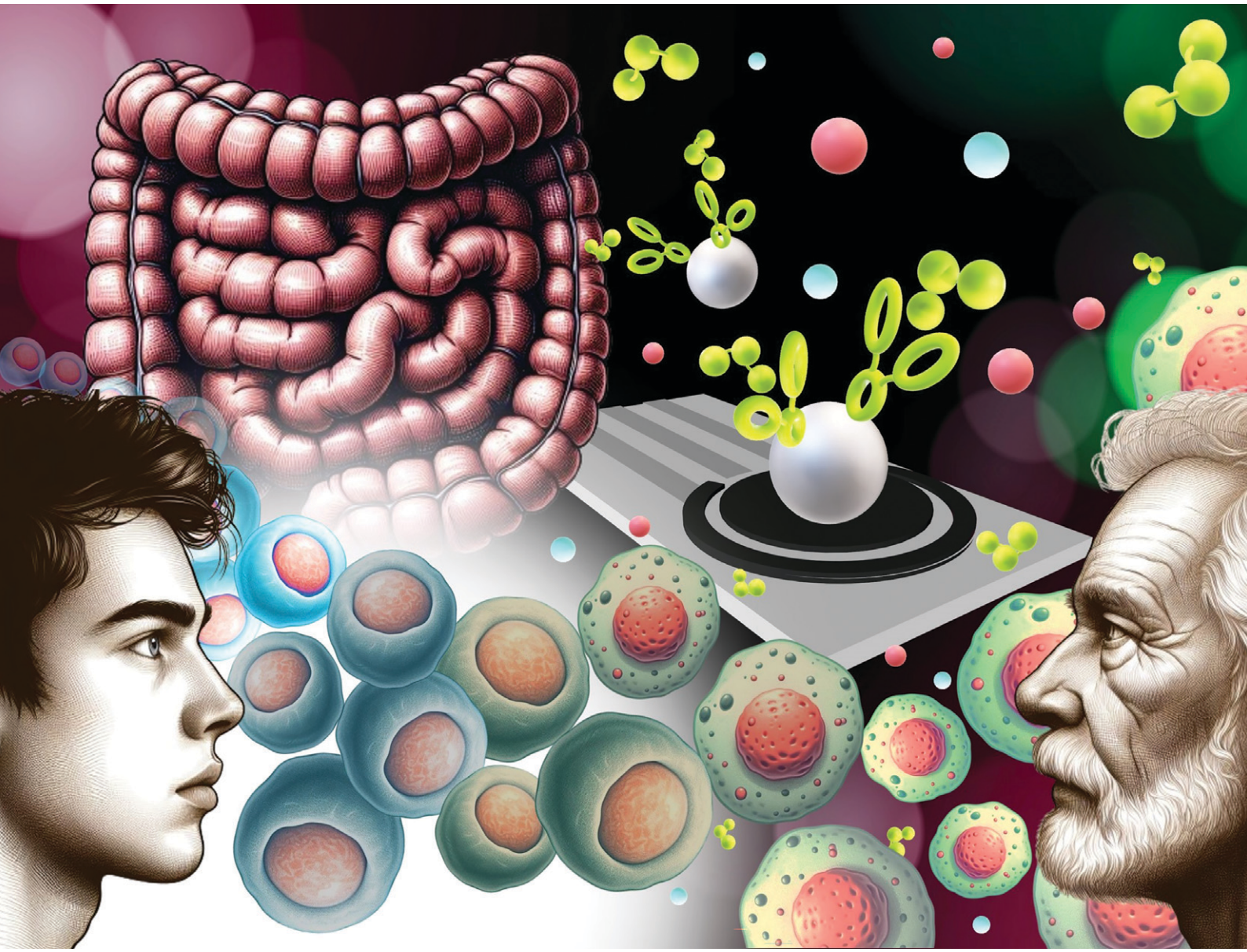

ISSN 2635-0998

ROYAL SOCIETY OF CHEMISTRY

PAPER
Rodrigo Barderas, Susana Campuzano *et al.*
Magneto-controlled electrochemical immunosensing platform to assess the senescence-associated GDF-15 marker in colorectal cancer

Sensors & Diagnostics

PAPER

View Article Online
View Journal | View Issue

Cite this: *Sens. Diagn.*, 2024, **3**, 238

Magneto-controlled electrochemical immunosensing platform to assess the senescence-associated GDF-15 marker in colorectal cancer†

Sandra Tejerina-Miranda,[a] Víctor Pérez-Ginés,[a] Rebeca M. Torrente-Rodríguez,[a] María Pedrero,[a] Ana Montero-Calle,[b] José M. Pingarrón,[a] Rodrigo Barderas*[b] and Susana Campuzano*[a]

In this study, we report a novel electrochemical immunoplatform using magnetic micro-supports and screen-printed carbon electrodes (SPCEs), overcoming limitations of the methods reported to date, for the rapid and sensitive determination of GDF-15, a molecular marker associated with cellular senescence in aging and cancer development and prognosis. The immunoplatform incorporated a sandwich-type configuration with specific capture and biotinylated-detection antibodies and used a streptavidin–peroxidase (strep–HRP) enzymatic conjugate as label. After magnetic capturing the micro-supports with the sandwich HRP-labeled immunocomplexes onto the surface of a SPCE, the change in cathodic current was quantified in the presence of H_2O_2 and hydroquinone (HQ), showing a direct correlation with the GDF-15 concentration. The proposed bioplatform exhibited attractive performance characteristics, including a good reproducibility (RSD 4.3%), and a wide linear concentration dynamic range from 140 to 10 000 pg mL^{-1} with a low limit of detection (LOD) of 42 pg mL^{-1} for GDF-15 standards in buffered solutions. The selectivity of the developed method and the storage stability of the capturing immunoconjugates were noteworthy. Indeed, the immunoconjugates showed a reliable performance for over 28 days when stored in a refrigerator. The immunoplatform was applied to a cohort of 19 plasma samples representing the different stages of colorectal cancer (CRC). The method allowed efficient discrimination between healthy individuals and CRC patients, particularly those in advanced stages, within a rapid 75-minute timeframe. The immunoplatform also presents substantial advantages in terms of cost-effectiveness, assay time reduction, and simplicity compared to other available techniques.

Received 21st November 2023,
Accepted 15th January 2024

DOI: 10.1039/d3sd00311f

rsc.li/sensors

Introduction

Cellular senescence is a complex state of stable cell cycle arrest in which proliferating cells become unresponsive to growth-promoting stimuli, which typically occurs in response to DNA damage.[1,2] Originally thought to be an artifact of cell culture, senescence has emerged as a crucial cellular defence mechanism against stress, playing diverse roles in physiological and pathological processes such as tissue remodelling, injury response, and cancer development.[3] One of its hallmarks is the senescence-associated secretory phenotype (SASP), which encompasses a wide range of soluble factors secreted by senescent cells.[4] SASP comprises a variety of cytokines, chemokines, growth factors, angiogenic factors, proteases, bioactive lipids, extracellular matrix components, and matrix metalloproteinases,[5] and has been shown to be associated with age-related health, mortality from cardiovascular diseases, several types of cancer, and Alzheimer's disease.[6,7]

Focusing on cancer, SASP has a paradoxical role that is still under investigation. On the one hand, it can prevent cell division and promote immune clearance of damaged cells, thus preventing the development of tumors[8] but, on the other hand, it can often promote resistance to treatment and cancer recurrence. When non-malignant senescent cells secrete SASP, tumorigenesis of premalignant cells can be driven, counteracting the overall beneficial effects of senescence.[6] Consequently, controlling SASP factors emerges as a

[a] *Departamento de Química Analítica, Facultad de CC. Químicas, Universidad Complutense de Madrid, Pza. de las Ciencias 2, 28040-Madrid, Spain. E-mail: susanacr@quim.ucm.es*
[b] *Chronic Disease Programme, UFIEC, Institute of Health Carlos III, Majadahonda, 28220-Madrid, Spain. E-mail: r.barderasm@isciii.es*

† Electronic supplementary information (ESI) available. See DOI: https://doi.org/10.1039/d3sd00311f

compelling strategy to manage cancer, with significant potential as biomarkers of senescence and prospects for clinical utility in the detection of cancer and metastasis.[7]

Colorectal cancer (CRC) is one of the most common – the third most diagnosed cancer in the world – and lethal – the third cause of cancer-related death and the second in men under 50 years.[9] Currently, there is a firm conviction that the determination of a specific set of biomarkers can decisively complement traditional methods to provide an earlier and more personalized diagnosis of this neoplasia with the advantages that this represents to improve the survival and quality of life of patients.[10]

Growth differentiation factor 15 (GDF-15, also known as macrophage inhibitory cytokine 1, MIC-1), belongs to the transforming growth factor β (TGF-β) cytokine superfamily.[11] GDF-15 is a widely distributed protein, which plays multiple roles in physiological and pathological conditions.[12] Its effects are pleiotropic, encompassing appetite regulation, actions on metabolism, pregnancy, cell survival, immune response, and inflammation.[12,13] GDF-15 also plays different roles in the pathophysiology of cardiovascular diseases, autoimmunity, diabetes, and cancer, including CRC. In this sense, GDF-15 is an integral component of SASP that contributes to various cellular processes associated with CRC progression, including inflammation, cell proliferation, apoptosis, and metastasis.[14–16] When specifically considering metastasis in CRC, GDF-15 plays an important role as an activator of the TGF-β signalling cascade.[17] This intricate and versatile signalling pathway regulates a wide range of cellular processes and holds promise as a target for anticancer drug development in both preclinical and clinical stages.[18] Among the processes under the regulation of the TGF-β signalling cascade is metastasis mediated by epithelial-mesenchymal transition (EMT), which is activated by GDF-15.[19,20] Therefore, GDF-15 dysregulation within the SASP framework underlines its relevance as a well-established biomarker for detecting and characterizing metastatic CRC.[15,21,22]

Considering the importance of GDF-15 in assessing the presence and progression of CRC, clinical research strives to develop simple, sensitive, accurate, and cost-effective methods to monitor this biomarker. Traditionally, immunohistochemistry[23] and blotting technologies[24] have been used for GDF-15 detection, deprived of quantitative ability. Subsequently, Enzyme-Linked Immunosorbent Assay (ELISA) methodologies entailing skilled personnel, relatively long assay durations and bulky plate readers,[25–27] and DNA amplification[28] have been employed for the determination of GDF-15. Recently, electrochemical immunosensors have been harnessed for GDF-15 quantification, leveraging their unique attributes of sensitivity and selectivity.[29–32] However, despite their remarkably low detection limits and demonstrated applicability to the analysis of serum samples for the diagnosis and prognosis of cardiovascular diseases (CVDs), these biosensors required the use of nanomaterials and lengthy manufacturing processes. Furthermore, the reported immunosensors for GDF-15 used glassy carbon electrodes (GCEs), whose use in electrochemical biosensing shows certain well-known limitations, such as susceptibility to fouling, incompatibility with miniaturization and multiplexing, and the requirement of exhaustive electrode surface pretreatment.[33–35]

These drawbacks can be overcome by working with screen-printed carbon electrodes (SPCEs) and profiting from the inherent benefits provided by micromagnetic supports in biosensing, derived from their high surface-to-volume ratio, easy manipulation through magnetic fields, and versatility in surface chemistry for bioconjugation and efficient target capture. These benefits lead to innovative biosensing strategies with higher simplicity, improved sensitivity and kinetics, and minimization of matrix effects, thus satisfying the sought-after demands for point-of-care applications.[36–40] Accordingly, we report here the first electrochemical immunoplatform involving micromagnetic supports for the determination of GDF-15. This immunoplatform involves a sandwich-type immunoassay, enzymatic labeling with HRP and amperometric transduction at SPCEs, and represents a competitive alternative to other available methodologies for the simple and rapid quantification of GDF-15. Unlike other electrochemical immunoplatforms reported for the determination of GDF-15, all of them using integrated formats and focused on cardiovascular diseases,[29–32] the developed immunoplatform was applied to the identification and prognosis of CRC through the analysis of plasma samples.

Experimental section

Apparatus and electrodes

Amperometric measurements were performed at room temperature with a CHI812B potentiostat provided with CHI1140A software. Screen-printed carbon electrodes (SPCEs, DRP110, 4 mm ∅) consisting of a three-electrode cell configuration with a carbon working electrode (WE), a carbon auxiliary electrode (AE) and an Ag pseudo-reference electrode (RE) were used as electrochemical platforms.

The SPCEs and their connecting cable (DRP-CAC), were acquired from Metrohm-DropSens. The SPCEs were placed in a homemade polymethylmethacrylate (PMMA) casing with an embedded Nd magnet (∅ 4 × 4 mm, AIMAN GZ), ensuring the capture of the modified microbeads (MBs) on the WE surface. The whole casing was immersed in a 10 mL glass electrochemical cell to carry out the amperometric detection.

A magnetic particle concentrator DynaMag-2 (Cat. No: 12321D, Dynabeads®, Invitrogen™ Thermo Fisher Scientific), a BioSan TS-100 uniform temperature incubator shaker (Thermo), a magnetic stirrer (Inbea), a Crison model Basic 20+ pH-meter, a vortex (Velp Scientifica) and an MPW-65R centrifuge from MPW (Med. Instruments) were also employed.

Reagents and solutions

Carboxylic acid-functionalized MBs (HOOC-MBs, Dynabeads™, Cat. No.: M-270, 2.8 μm ∅, ~2 × 10^9 beads mL^{-1}) were purchased from Invitrogen™ Thermo Fisher Scientific. Commercial Blocker™ Casein in PBS (BB) was obtained from Thermo Scientific (Cat. No. 37528). Ethanolamine (ETA), hydroquinone (HQ), hydrogen peroxide (H_2O_2, 30% v/v), *N*-(3-dimethyl-aminopropyl)-*N*′-ethyl-carbodiimide (EDC) and *N*-hydroxysulfosuccinimide (sulfo-NHS) were acquired from Sigma-Aldrich.

Tris-hydroxymethyl-aminomethane-HCl (Tris-HCl), potassium chloride, sodium chloride, sodium di-hydrogen phosphate, di-sodium hydrogen phosphate and 2-(*N*-morpholino) ethanesulfonic acid (MES) were purchased from Scharlab. All used reagents were of the highest available grade.

Deionized water type I from a Millipore Milli-Q purification system (18.2 MΩ cm) was used for the preparation of all buffer solutions: 0.1 mol L^{-1} phosphate buffer (PB) solution pH 8.0; 0.1 mol L^{-1} Tris-HCl pH 7.2; 0.025 mol L^{-1} MES buffer pH 5.0; 0.01 mol L^{-1} phosphate buffer saline solution (PBS) pH 7.4 and 0.05 mol L^{-1} PB solution pH 6.0. For the activation and the blocking step of the HOOC-MBs an EDC/sulfo-NHS mixture solution (50 mg mL^{-1} each) prepared in MES buffer pH 5.0 and a 1.0 M ethanolamine (ETA) solution prepared in 100 mM PB buffer pH 8.0 were used, respectively. For the amperometric measurements, solutions of 100 mM HQ and 100 mM H_2O_2 were freshly prepared in 50 mM PB pH 6.0 just before their use.

The standard and the antibody pair used for the determination of Human GDF-15 were those provided in the commercial ELISA kit Human GDF-15 DuoSet ELISA (Cat. No. DY957, from R&D Systems) containing a Recombinant Human GDF-15 Standard, a Mouse Anti-Human GDF-15 Capture Antibody (CAb) and a Biotinylated Goat Anti-Human GDF-15 Detection Antibody (b-DAb). Streptavidin–HRP (strep–HRP) conjugate from Roche (Cat. No. 11089153001) was employed as enzymatic tracer.

IgG from human serum (hIgG, Cat. No. I2511), albumin from human serum (HSA, Cat. No. A1653), human haemoglobin (Hb, Cat. No. H7379), all from Sigma-Aldrich, and human TNFα (Cat. No. DY210) from R&D Systems, were assessed as potential interferents.

Sandwich immunoassay implementation on MBs

MBs modification was performed using 1.5 mL microcentrifuge tubes employing successive incubation and washing steps. Incubation steps were carried out using 25 μL of the corresponding solution in a thermoshaker at 25 °C under constant stirring (950 rpm). On the other hand, washing steps were done with 50 μL of the required solution. After each step, the microcentrifuge tube with the MBs suspension was placed in the magnetic separator for 2 min with the subsequent removal of the supernatant.

For each measurement, a 3 μL-aliquot of the HOOC-MBs suspension was placed in a 1.5 mL microcentrifuge tube and washed twice with MES buffer for 10 min. Subsequently, the carboxylic groups on the MBs surface were activated by incubation with freshly prepared EDC/sulfo-NHS solution for 35 min. After activation of the carboxylic groups, two washing steps were performed with MES buffer.

Thereafter, the activated HOOC-MBs were incubated for 45 min in a 25 μg mL^{-1} CAb solution prepared in MES buffer. The CAb-MBs were washed twice with the same buffer and incubated in 1.0 M ETA solution for 60 min to deactivate the remaining groups after CAb immobilisation. Then, the modified MBs were washed with 0.1 M Tris-HCl buffer (pH 7.2) and twice with 0.01 M PBS pH 7.4. The CAb-MBs were used for the measurements at the time of preparation or stored (in filtered PBS, at 4 °C) for later use.

For the determination of GDF-15, HRP-labeled sandwich immunocomplexes were formed upon three successive incubation steps: in the standard target protein solution (in PBS pH 7.4) for 15 min; then in a 0.5 μg mL^{-1} solution (in BB) of b-DAb for 30 min; and in a 1/1000 strep–HRP solution (in BB) for 30 min.

The resulting magnetic bioconjugates were washed twice with BB and re-suspended in 50 μL of PB pH 6.0 to perform the amperometric measurements.

Amperometric measurements

First, the SPCE was placed in the Nd-embedded-PMMA casing. Then, 50 μL of the MBs suspension were disposed on the surface of the WE of the SPCE (a new one was used for each determination).

The SPCE/PMMA casing set was connected to the potentiostat through the cable and immersed into a measuring cell containing 10 mL of PB buffer pH 6.0 and 100 μL of freshly prepared 0.1 mol L^{-1} HQ solution. Amperometric detection was made by applying continuous stirring and a constant potential of −0.20 V *vs.* the Ag pseudo-reference electrode.

Once the background current was stabilized, 50 μL of a freshly prepared 0.1 mol L^{-1} H_2O_2 were added to the electrochemical cell producing a cathodic current variation due to the HQ-mediated enzymatic reduction of H_2O_2. The signals given in the manuscript were calculated as the difference between the steady-state current (after H_2O_2 addition) and the background current (before H_2O_2 addition) and are the mean values resulting from three replicates. The error bars were calculated as the standard deviation (SD) of these replicates.

Analysis of plasma samples

Plasma samples from patients with CRC and healthy individuals were provided by the biobank of the San Carlos Clinical Hospital after approval by the Ethical Review Committee (CEI PI 45). These samples, stored at −80 °C, were handled and used anonymously accomplishing all the ethical

issues. Experiments were performed in agreement with relevant guidelines and regulations of Hospital Universitario Clínico San Carlos, Instituto de Salud Carlos III and Universidad Complutense de Madrid. All individuals provided written informed consent for the use of their biological samples for research purposes, adhering to ethical principles outlined by Spain (LOPD 15/1999) and the European Union Fundamental Rights of the EU (2000/C364/01).

Although no matrix effect was observed when analysing 25 times diluted plasma samples, considering the low content of the target protein, the determination was performed employing standard additions calibration plots for GDF-15 with concentrations between 0 and 5000 pg mL^{-1}.

Results and discussion

This work reports the first electrochemical immunoassay involving micromagnetic supports and SPCEs for the determination of GDF-15. The bioplatform entails efficient capture of the target protein, GDF-15, through a specific antibody (CAb) onto the surface of HOOC-MBs. Subsequently, GDF-15 is sandwiched using a biotinylated detector antibody (b-DAb) and further enzymatically labeled with a streptavidin–horseradish peroxidase (strep–HRP) conjugate. Upon magnetic capture of the MBs bearing the immunoconjugates onto the surface of the SPCEs, electrochemical detection is performed by monitoring the cathodic current measured at −0.20 V *vs.* the Ag pseudo-reference electrode utilizing the H_2O_2/HQ system. The design of the immunoplatform and the reactions involved in the amperometric transduction are illustrated in Scheme 1.

Optimization of experimental variables

In seeking to optimize the effectiveness of our proposed immunodetection strategy, a comprehensive evaluation of each operational parameter, which directly impacts its proper functioning, was undertaken. The selection criterion for this evaluation was based on attaining the utmost signal-to-blank ratio (S/B) under two conditions: the absence (B) and the presence (S) of 1000 pg mL^{-1} GDF-15 standard. A graphical display of the evaluated variables, their corresponding ranges, and the selected values are shown and summarized in Fig. 1 and Table 1, respectively. Other experimental parameters, such as the quantity of HOOC-MBs utilized per determination and all the factors associated with the

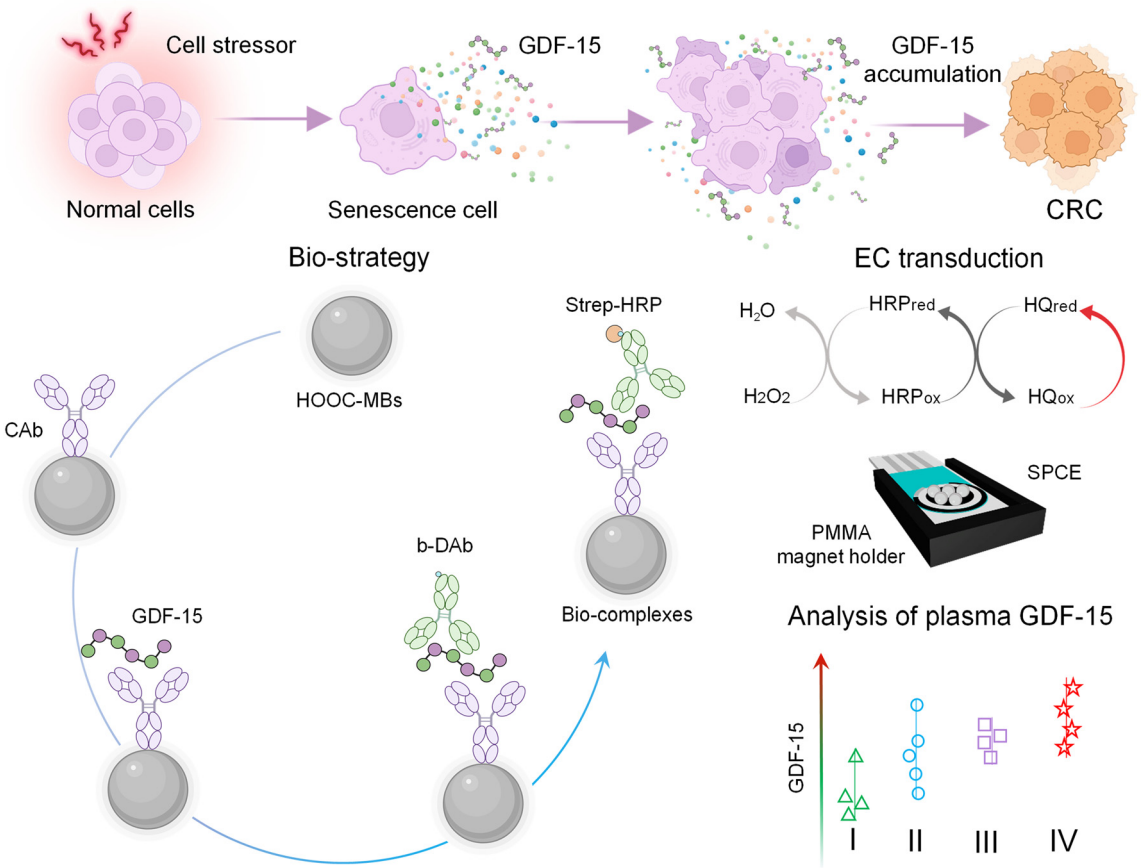

Scheme 1 Schematic diagram showing the steps involved in the preparation of GDF-15 sandwich immunocomplexes on HOOC-MBs, the amperometric transduction of the resulting magnetic bioconjugates at a SPCE in the presence of H_2O_2 and HQ, and the main application of the developed bioplatform. Created with Biorender.

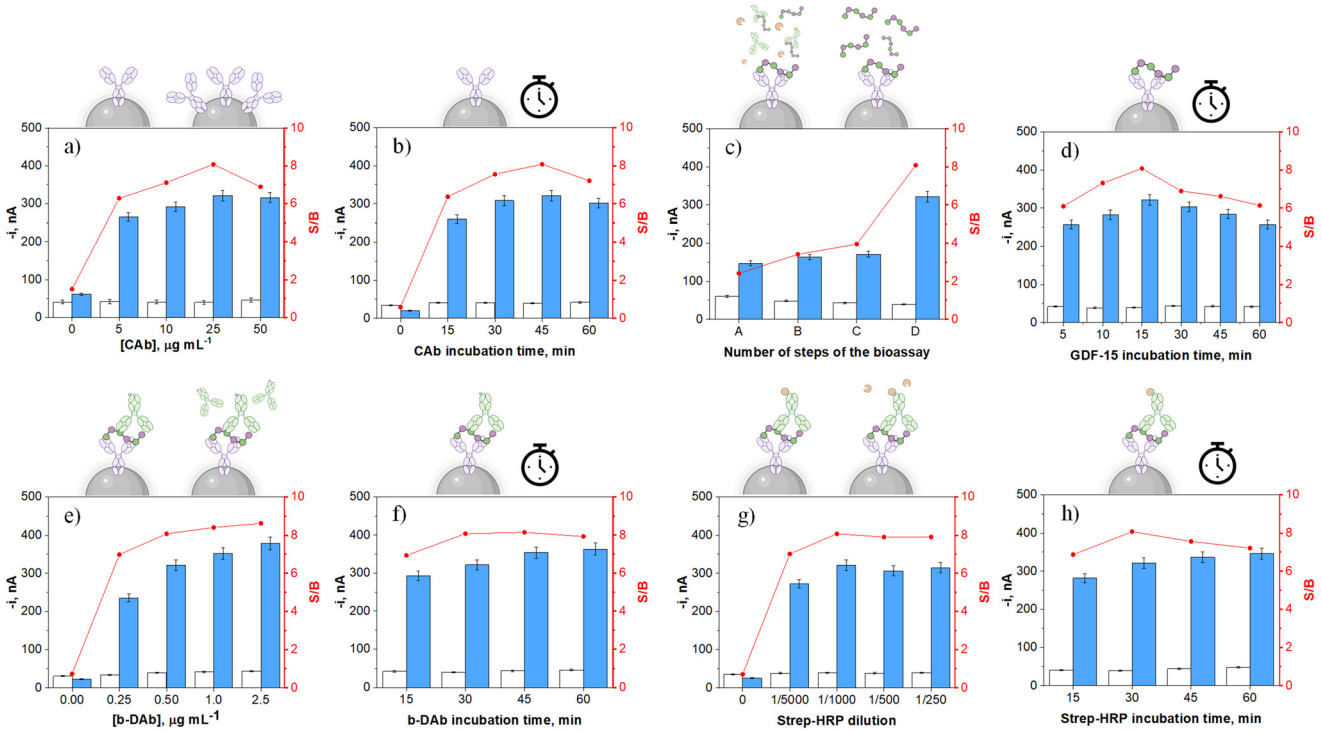

Fig. 1 Dependence of the amperometric responses obtained with the developed immunoplatform in the absence (B, white bars) and in the presence (S, blue bars) of 1000 pg mL^{-1} GDF-15, concerning the following variables: (a) CAb concentration and (b) incubation time, (c) number of steps involved in the assay (see main text for A–D symbols meaning), (d) target GDF-15 incubation time, (e) b-DAb concentration and (f) incubation time, (g) strep–HRP conjugate dilution, and (h) incubation time. The resulting S/B ratios are represented by red dots and lines.

amperometric transduction, were optimized in previous studies.[41,42]

Fig. 1a and b show higher S/B ratios for MBs incubated in a 25 μg mL^{-1} CAb solution for 45 min. The decreases observed for larger concentrations and longer incubation times were attributed to smaller S responses, probably due to hindered target recognition by CAb crowding.[43] Furthermore, as multiple steps are involved in forming sandwich immunocomplexes on the surface of CAb-MBs, it is important to check how the used protocol (*i.e.*, the number of involved steps) influences the measurements. Four different protocols, all starting from the CAb-MBs preparation and involving different 30 min incubation steps using single or mixture solutions of the bioreagents employed for the formation of the HRP-labeled sandwich immunocomplexes, have been evaluated as detailed in Table 2.

As Fig. 1c shows, the specific signal in the presence of GDF-15 achieved a larger value with the 3-step protocol (D) involving the sequential incubation of CAb-MBs with the target protein, b-DAb, and the enzymatic tracer strep–HRP solutions, respectively. Conversely, the incubation of CAb-MBs immunoconjugates with mixtures of GDF-15 and b-DAb (protocol B), b-DAb and strep–HRP (protocol C), or GDF-15, b-DAb, and strep–HRP (protocol A) resulted in lower S responses, suggesting poorer GDF-15 capture and/or labeling efficiencies. Therefore, 15 min was selected as the incubation time of CAb-MBs with the target antigen (Fig. 1d). In addition, according to Fig. 1e, the S/B ratio exhibited an ascending trend with increasing b-DAb concentration. Nevertheless, since this trend is not pronounced, 0.5 μg mL^{-1}

Table 1 Summary of the optimized experimental parameters employed in the construction of the MBs-assisted immunoplatform for the determination of GDF-15

Variable		Studied range	Selected value
Number of steps		1–3	3
Concentrations, μg mL^{-1}*/dilution**	CAb*	0.0–50.0	25.0
	b-DAb*	0.0–2.5	0.5
	Strep–HRP**	0–1/250	1/1000
Incubation times, min	CAb	0–60	45
	GDF-15	5–60	15
	b-DAb	15–60	30
	Strep–HRP	15–60	30

Table 2 Protocols evaluated for assembling HRP-labeled sandwich immunocomplexes on CAb-MBs

Protocol	Successive incubation steps (30 min each)			Assay time, min
	GDF-15	b-DAb	Strep–HRP	
A	1			30
B	1		2	60
C	1	2		60
D	1	2	3	90

b-DAb was chosen for further work to avoid an unnecessary cost increase per determination.

Fig. 1g shows as a larger S/B ratio was obtained with a 1/1000 dilution of the strep–HRP conjugate. It is important to note that bars 0 in Fig. 1a, e and g confirmed the need of using the three bioreagents to carry out the assay which took place through the formation of sandwich-type immune complexes labeled with HRP. These results also confirmed the effectiveness of the blocking step after CAb immobilization on MBs, which effectively prevented nonspecific adsorption of b-DAb or strep–HRP in the absence of GDF-15.

Considering the incubation times for b-DAb and strep–HRP conjugate (Fig. 1f and h), it was seen that 30 min incubations were adequate for GDF-15 sandwiching and enzymatic labeling, respectively, since incubation times did not significantly improve the S/B ratios. Using the optimized conditions, it is important to highlight that, counting from the deactivated CAb-MBs, the determination of GDF-15 can be completed in as short time as 75 min.

Analytical and operational characteristics

Under the optimized working conditions summarized in Table 1, a calibration plot was constructed for GDF-15 standards in buffered solutions. As it can be seen in Fig. 2, a linear calibration plot (r = 0.996) was obtained over the 140–10 000 pg mL^{-1} GDF-15 concentration range, fitting the equation – i, nA = (0.236 ± 0.005) nA mL pg^{-1} [GDF-15] + (56 ± 21) nA. The limit of detection (LOD) and quantification (LOQ) values were estimated using, respectively, the 3 × s_b/slope and 10 × s_b/slope criteria (s_b: standard deviation of ten amperometric measurements in the absence of GDF-15).[44–46] The obtained values were 42.0 and 140.0 pg mL^{-1}, respectively.

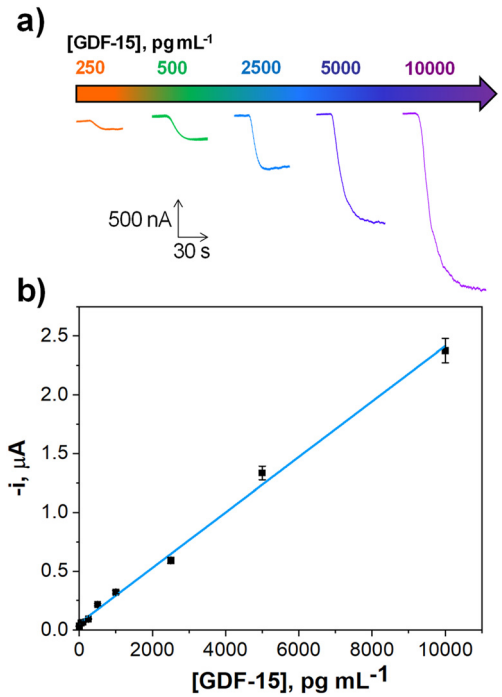

Fig. 2 Actual amperometric traces recorded at the indicated concentrations (a) and calibration graph (b) constructed for the determination of GDF-15 with the developed immunoplatform.

It is important to highlight the low LOD achieved by the bioplatform, considerably lower than the cut-off values established for GDF-15 in serum samples to identify CRC patients (around 1000 pg mL^{-1}).[14,47]

The reproducibility of the measurements and the storage stability of the CAb-MBs were evaluated. The responses for 1000 pg mL^{-1} GDF-15 measured with ten different bioplatforms prepared the same day, gave a relative standard deviation (RSD) value of 4.3%. This result highlights both the reproducibility of the methodology used to implement the sandwich-type immunoassay on the MBs, and that of the amperometric measurements. Furthermore, the amperometric responses provided in the absence and in the presence of 2500 pg mL^{-1} GDF-15 by immunoplatforms constructed using the stored CAb-MBs (at 4 °C resuspended in filtered PBS) were compared. The results obtained (Fig. S1 in the ESI†) showed that the as prepared immunoplatforms gave similar S/B values for at least 28 days after the CAb-MBs preparation.

Table S1 (in the ESI†) summarizes the most relevant characteristics of other electrochemical immunosensors recently reported in the literature for the determination of GDF-15.

As it can be seen, the reported immunosensors[29–32] claimed lower LOD values than that achieved with the developed immunoplatform. However, all of them involved complex, long, and laborious protocols for their preparation and used nanomaterials. Therefore, although the developed immunoplatform, provides a slightly lower detectability, but, nevertheless, able to respond to the demands of the clinic, it is attractive in terms of simplicity, preparation and testing time and use of disposable substrates, thus exhibiting advantages for its potential future implementation in POC and/or multiplexing devices. It is also important to note that all the reported immunosensors were applied for cardiovascular diseases, thus leaving unexplored the possibility of using GDF-15 in the diagnosis and prognosis of other diseases of high prevalence and mortality such as CRC.

On the other hand, the comparison of the linear ranges of the bioplatform and those specified in the commercial ELISA kit that uses the same immunoreagents (DY957 DuoSet ELISA, R&D Systems, 7.8–500 pg mL^{-1}), and taking into account that the bioplatform uses a standard/sample volume 4 times lower (25 *vs.* 100 µL) both technologies offer similar sensitivity but the electrochemical biotool is attractive for point-of-care applications and even home testing, due to the requirement of cost-effectiveness, simple and portable instrumentation.

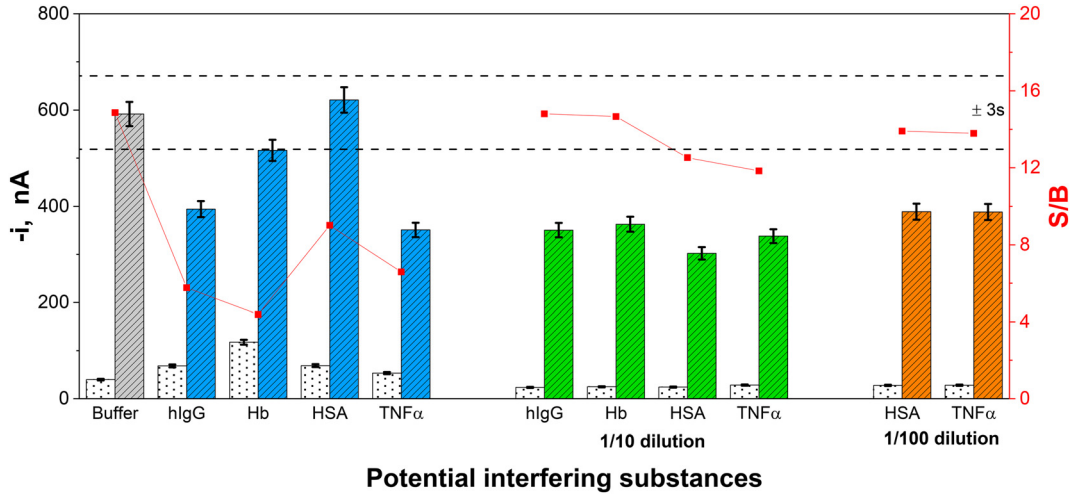

Fig. 3 Amperometric responses provided by the developed bioplatform for 0 (dotted bars) and 2500 pg mL^{-1} GDF-15 (striped bars) standards prepared in the absence and in the presence of 1 or 0.1 mg mL^{-1} hIgG, 5 or 0.5 mg mL^{-1} Hb, 50, 5.0 or 0.5 mg mL^{-1} HSA and 10, 1.0 or 0.1 ng mL^{-1} TNFα. S/B ratio values were displayed using red dots, whereas control limits (dashed black lines) were set at three times the standard deviation of the S/B mean value of three measurements obtained in the absence of interferent.

Selectivity

To glimpse whether there would be interferences when applying the developed immunoplatform to real samples, the effect of the following proteins found in human serum, hIgG, HSA, Hb and TNFα, was evaluated. Therefore, the effect of diluted solutions of these potential interfering proteins (at the concentration levels reported in healthy individuals and indicated in Fig. 3 caption) on the amperometric signals recorded in the absence and in the presence of 2500 pg mL^{-1} GDF-15, was checked.

Furthermore, the supplier company of the employed immunoreagents (DY957 DuoSet ELISA, R&D Systems) certified no cross-reactivity for recombinant human GDF-11, for recombinant mouse GDF-5, GDF-6, GDF-7, GDF-8 and Pro-GDF-8, all of them prepared at a 50 ng mL^{-1} concentration.

As can be seen in Fig. 3, the four tested proteins interfered with the determination of GDF-15 at the largest concentrations tested.

The interference of hIgG, Hb and HSA is widely described in the literature; hIgG interference can be attributed both to its nonspecific adsorption on the surface of MBs[48] and to the presence of circulating human antibodies which can react with mouse-expressed antibodies, as it is the CAb involved in the developed immunoplatform, leading to inaccurate results.[49] The interference observed for Hb, which significantly affects the amperometric response in the absence of GDF-15, can be attributed to its peroxidase activity which has been widely reported to cause false positives.[50] The interference from HSA, especially when used at concentrations equal to or larger than 5 mg mL^{-1}, has been mainly attributed to the presence of IgG in low-purity HSA lots.[49,51] The interference observed for TNFα is not so well described in the literature as that for the other tested proteins. This interference can be attributed to interaction with the target proteins or to nonspecific recognition by the used antibodies. A hypothesis that may justify this result is the tendency of TNFα to form clusters that can somehow trap the target protein, preventing its recognition.[52]

As expected, an appropriate dilution of these four non-target proteins (10 times for hIgG and Hb, and 100 times for HSA and TNFα) provoked minimization of their interference.

Analysis of plasma samples

The designed immunoplatform was used for the analysis of 19 plasma samples from healthy individuals (4) and from CRC patients (15) diagnosed at different stages of the disease (I–IV).

The possible existence of a matrix effect was evaluated by comparing the slope values of the calibration plot constructed for GDF-15 in buffer solution with those prepared in 25-fold diluted solutions of representative plasma samples from a healthy subject and a stage IV CRC patient.

No statistically significant differences were found between the slope values of the calibration plots constructed with GDF-15 standards prepared in buffered solutions ((0.24 ± 0.01) nA mL pg^{-1}) and in 25-fold diluted plasma samples from healthy individuals ((0.25 ± 0.01) nA mL pg^{-1}) and CRC patients ((0.24 ± 0.01) nA mL pg^{-1}), t_{exp} values of 0.219 and 0.012, respectively, which are lower than t_{tab} = 4.303 (n = 3, α = 0.05).[53] Therefore, under the mentioned conditions, no matrix effect was apparent. However, the low target protein content in the diluted samples led us to carry out the determination by applying the standard additions method through the supplementation of 25-diluted plasma samples with increasing concentrations of GDF-15, from 0 to 5000 pg mL^{-1}. The obtained results are displayed in Fig. 4, where the

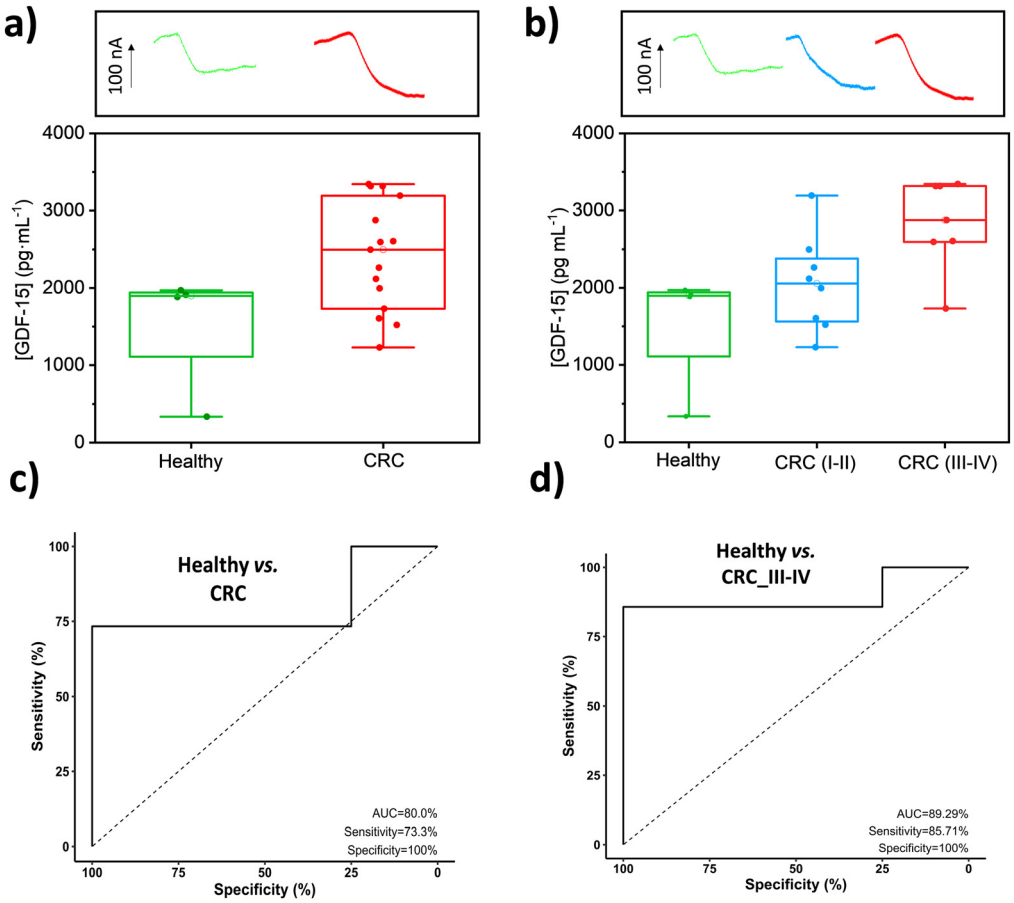

Fig. 4 GDF-15 concentrations found by the bioplatform in plasma samples grouped into pools of healthy individuals and patients with CRC (a) and healthy and patients with CRC diagnosed in early (I and II) or advanced (III and IV) stages (b). Above (a) and (b) real amperometric responses provided by the developed bioplatform in the analysis of plasma samples representative of each type of tested individuals. ROC curves to discriminate healthy individuals from patients with CRC (c) and healthy individuals from patients with CRC in advanced stages (III and IV) (d).

concentrations found for healthy individuals (healthy group), for CRC patients (CRC group) and for CRC patients at early stages of the disease (CRC (I and II) group) and at advanced stages of the disease (CRC (III and IV) group), are compared.

These results confirmed larger GDF-15 plasmatic concentrations in CRC patients (range 1229–3342 pg mL^{-1}, mean 2413.7 pg mL^{-1}) compared to healthy subjects (range 337–1971 pg mL^{-1}, mean 1525.6 pg mL^{-1}) and, within the former, larger at advanced stages (III–IV: 1732–3342 pg mL^{-1}, mean 2826.2 pg mL^{-1}) than at early stages (I–II: 1229–3193 pg mL^{-1}, mean 2052.8 pg mL^{-1}). This agrees with the gradual increase reported in the serological concentration of GDF-15 with the subsequent stages of CRC advancement.[54,55] These results are perfectly in line with the valuable potential of GDF-15 for CRC detection and prognosis.[14,17,20,21,22,47,56–60] Indeed, it has been reported that GDF-15 levels in serum gradually increase in the process of conversion from adenomatous polyps to colorectal carcinoma[14,59] and that CRC patients with an increased serum level of GDF-15 had a 2.09-fold higher risk of death[11] and worse cancer-specific survival (CSS).[21] In our results, this would correspond to the CRC plasma samples at advanced stages (1.85-fold higher GDF-15 plasma values than healthy individuals). It is also important to note that the concentration ranges found with the bioplatform in the explored cohort agree with those reported in the literature for healthy subjects: (427–851 pg mL^{-1}),[61] (167.9–1203.9 pg mL^{-1}),[14] (33.9–2398.9 pg mL^{-1})[47] and CRC patients: (908–3152 pg mL^{-1}),[61] (240.1–3713.4 pg mL^{-1})[14] and (112.0–5178 pg mL^{-1}).[47]

Table 3 Potential of plasma GDF-15 level determined with the bioplatform to diagnose and prognose CRC

Parameter	Healthy *vs.* CRC	Healthy *vs.* CRC III and IV
AUC (%)	80.0	89.3
Sensitivity (%)	73.3	85.7
Specificity (%)	100.0	100.0
Cut-off, pg mL^{-1}	1983.5	2283.0

In addition, a more exhaustive analysis of the results provided by the developed bioplatform using ROC curves (Fig. 4c and d, Table 3) shows its potential to discriminate between healthy individuals and CRC patients, and particularly between healthy subjects and CRC patients with advanced stages (III and IV), yielding the plasma cut-off

values of GDF-15 that are also included in the Table and allow these discriminations. These results agree with the role of GDF-15 as a negative prognostic marker in CRC whose elevated plasma levels correlate with increased risk of recurrence and reduced overall survival.[44,55]

In addition, the accuracy of the results provided by the bioplatform in the analysis of plasma samples was evaluated by performing recovery studies. A representative sample of each pool (healthy, CRC I, CRC II, CRC III, and CRC IV) was spiked with 1000 pg mL^{-1} GDF-15 standard. The obtained results, using the same protocol as for non-supplemented samples and upon the subtraction of the endogenous content found in each sample from the overall concentration determined after sample spiking, provided recovery values between 100 and 106% for the 5 types of samples analyzed, thus confirming the accuracy of the methodology.

Conclusions

This article reports the first electrochemical immunoplatform for the determination of GDF-15 employing HRP-labeled sandwich immunocomplexes linked to the surface of MBs captured on SPCEs for amperometric transduction.

The developed bioplatform exhibits analytical (LOD considerably lower than the cut-off value established in serum to diagnose several types of cancer) and operational characteristics compatible with its clinical application. The developed bioplatform has been tested for 19 plasma samples of healthy individuals and CRC patients at different stages of the disease. The results show its potential for a minimally invasive diagnosis and prognosis in only 75 min and using a minimum amount of sample (1 μL plasma/determination).

This new biotool represents an attractive alternative to conventional technologies (blotting and ELISA), as well as to other recently described electrochemical immunosensors, for the simple, rapid, and point-of-need determination of GDF-15. These features, together with the demonstrated applicability and compatibility with integration in multiplexing devices, offer it as a tool to help understanding GDF-15 regulation and expression in metastatic colon cancer and therefore providing more reliable diagnoses and prognoses of this neoplasm. Furthermore, considering that recent literature reports that GDF-15 promoted 5-Fluorouracil (5-FU, the conventional chemotherapeutic in CRC treatment) resistance, its determination can contribute to both precision medicine and therapy.[60,62]

Conflicts of interest

The authors declare no conflict of interest.

Acknowledgements

The financial support of Grant PID2019-103899RB-I00 funded by MCIN/AEI/10.13039/501100011033, EU's Horizon 2020 funding programme (UCM's Specific Research Fund FEI-EU-22-08) and PI20CIII/00019 and PI23CIII/00027 grants from the AES-ISCIII Program co-founded by FEDER funds are gratefully acknowledged.

References

1 F. d'Adda di Fagagna, *Nat. Rev. Cancer*, 2008, **8**(7), 512–522.
2 R. Shmulevich and V. Krizhanovsky, *Antioxid. Redox Signaling*, 2021, **34**(4), 324–334.
3 D. Paramos-De-Carvalho, A. Jacinto and L. Saúde, *eLife*, 2021, **10**, e72449.
4 N. Ohtani, *Inflammation Regener.*, 2022, **42**, 11.
5 R. Kumari and P. Jat, *Front. Cell Dev. Biol.*, 2021, **9**, 645593.
6 M. Takasugi, Y. Yoshida, E. Hara and N. Ohtani, *FEBS J.*, 2022, **290**(5), 1348–1361.
7 A. Domen, C. Deben, J. Verswyvel, T. Flieswasser, H. Prenen, M. Peeters, F. Lardon and A. Wouters, *J. Exp. Clin. Cancer Res.*, 2022, **41**, 360.
8 J. Yang, M. Liu, D. Hong, M. Zeng and X. Zhang, *Front. Cell Dev. Biol.*, 2021, **9**, 722205.
9 R. L. Siegel, N. Sandeep Wagle, A. Cercek, R. A. Smith and A. Jemal, *Ca-Cancer J. Clin.*, 2023, **73**, 233–254.
10 X. Hua, M. Kratz, R. C. Malen, J. Y. Dai, S. Lindström, Y. Zheng and P. A. Newcomb, *Br. J. Cancer*, 2021, **125**(6), 806–815.
11 L. N. Lawton, M. F. Bonaldo, P. C. Jelenc, L. Qiu, S. A. Baumes, R. A. Marcelino, G. M. de Jesus, S. Wellington, J. A. Knowles, D. Warburton, S. Brown and M. B. Soares, *Gene*, 1997, **203**, 17–26.
12 A. Assadi, A. Zahabi and R. A. Hart, *Pflugers Arch.*, 2020, **472**, 1535–1546.
13 P. Iglesias, R. A. Silvestre and J. J. Díez, *Endocrine*, 2023, **81**, 419–431.
14 C. Li, X. Wang, J. I. Casal, J. Wang, P. Li, W. Zhang, E. Xu, M. Lai and H. Zhang, *J. Cell. Mol. Med.*, 2016, **20**(8), 1420–1426.
15 M. Vocka, D. Langer, J. Petryl, M. Kalousová, T. Zima, T. Hanuš and L. B. Petruzelka, *J. Clin. Oncol.*, 2016, **34**(15_suppl), e15098.
16 S. J. Baek and T. E. Eling, *Pharmacol. Ther.*, 2019, **198**, 46–58.
17 C. Li, J. Wang, J. Kong, J. Tang, Y. Wu, E. Xu, H. Zhang and M. Lai, *Oncotarget*, 2015, **7**(1), 860–872.
18 A. B. Baba, B. Rah, G. M. Bhat, I. Mushtaq, S. Parveen, R. Hassan, M. H. Zargar and D. Afroze, *Front. Pharmacol.*, 2022, **13**, 791272.
19 J. Xu, S. Lamouille and R. Derynck, *Cell Res.*, 2009, **19**(2), 156–172.
20 Y. Zhang, X. Wang, M. Zhang, Z. Zhang, L. Jiang and L. Li, *Biotechnology*, 2018, **46**(sup2), 652–658.
21 Y. Wang, T. Jiang, M. Jiang and G. Shuijing, *BMC Cancer*, 2019, **19**, 177.
22 J. Robotycka, S. Mielcarska, M. Dawidowicz, A. Kula, B. Ochman, T. Niebudek, B. Strzałkowska, D. Waniczek and E. Świętochowska, *Med. Res. J.*, 2022, **7**(3), 208–214.
23 K. Souček, A. Malenovská, Z. Kahounová, J. Remšík, Z. Holubcová, T. Soukup, D. Kurfürstová, J. Bouchal, T.

Suchánková, E. Slabáková and A. Hampl, *J. Assist. Reprod. Genet.*, 2018, **35**(8), 1407–1417.
24 P. J. Emmerson, K. L. Duffin, S. Chintharlapalli and X. Wu, *Front. Physiol.*, 2018, **9**, 1712.
25 J. Trovik, H. B. Salvesen, T. Cuppens, F. Amant and A. C. Staff, *Int. J. Gynecol. Cancer*, 2014, **24**(2), 252–259.
26 Y. Zhang, W. Jiang, L. Wang and K. Lingappan, *Toxicol. Appl. Pharmacol.*, 2017, **332**, 8–14.
27 K. Liu, B. Liu, G. A. Wittert, C. Thompson, A. T. Hutchison and L. K. Heilbronn, *Obes. Res. Clin. Pract.*, 2023, **17**(1), 91–93.
28 T. Ebai, F. M. S. De Oliveira, L. Löf, L. Wik, C. Schweiger, A. Larsson, U. Keilholtz, J. Haybaeck, U. Landegren and M. Kamali-Moghaddam, *Clin. Chem.*, 2017, **63**(9), 1497–1505.
29 M. Chen, L. Zhao, D. Wu, S. Tu, C. Chen, H. Guo and Y. Xu, *Anal. Chim. Acta*, 2022, **1223**, 340194.
30 Y. Jiao, Z. Huang, M. Chen, X. Zhou, H. Lu, B. Wang and X. Dai, *Anal. Methods*, 2022, **14**, 1420–1429.
31 C. Chen, J. Kang, S. Wang, S. Chen, H. Guo and M. Chen, *Microchim. Acta*, 2023, **190**, 92.
32 M. Chen, Y. Jiao, C. Chen, Y. Wang, H. Lu and X. Dai, *Microchem. J.*, 2023, **193**, 109150.
33 A. M. Abdel-Aziz, H. H. Hassan and I. H. A. Badr, *Anal. Chem.*, 2020, **92**(11), 7947–7954.
34 E. Sramkova, T. Bystron and K. Bouzek, *Electrochim. Acta*, 2021, **379**, 138177.
35 M. Devi, M. Vomero, E. Fuhrer, E. Castagnola, C. Gueli, S. Nimbalkar, M. Hirabayashi, S. Kassegne, T. Stieglitz and S. Sharma, *J. Neural Eng.*, 2021, **18**(4), 041007.
36 W. Lai, D. Tang, J. Zhuang, G. Chen and H. Yang, *Anal. Chem.*, 2014, **86**, 5061–5068.
37 Y. Lin, Q. Zhou, J. Li, J. Shu, Z. Qiu, Y. Lin and D. Tang, *Anal. Chem.*, 2016, **88**, 1030–1038.
38 B. A. Otieno, C. E. Krause and J. F. Rusling, *Methods Enzymol.*, 2016, **571**, 135–150.
39 S. Fortunati, C. Giliberti, M. Giannetto, A. Bertucci, S. Capodaglio, E. Ricciardi, P. Giacomini, V. Bianchi, A. Boni, I. De Munari, R. Corradini and M. Careri, *Biosens. Bioelectron.: X*, 2023, **15**, 100404.
40 S. Fortunati, M. Giannetto, C. Giliberti, M. Mattarozzi, A. Bertucci and M. Careri, *Analysis Sensing*, 2023, e202300062.
41 M. Eguílaz, M. Moreno-Guzmán, S. Campuzano, A. González-Cortés, P. Yáñez-Sedeño and J. M. Pingarrón, *Biosens. Bioelectron.*, 2010, **26**(2), 517–522.
42 F. Conzuelo, M. Gamella, S. Campuzano, D. G. Pinacho, A. Reviejo, M. P. Marco and J. M. Pingarrón, *Biosens. Bioelectron.*, 2012, **36**(1), 81–88.
43 D. M. Kim, X. T. Yao, R. Vanam and M. S. Marlow, *mAbs*, 2019, **11**(7), 1319–1330.
44 K. Hasebe and J. Osteryoung, *Anal. Chem.*, 1975, **47**, 2412.
45 L. H. Keith, W. Crummett, J. Deegan Jr., R. A. Libby, J. K. Taylor and G. Wentler, *Anal. Chem.*, 1983, **55**, 2210–2218.
46 P. Borman and D. Elder, Q2(R1) validation of analytical procedures: text and methodology, *ICH quality guidelines: an implementation guide*, ed. A. Teasdale, D. Elder and R. W. Nims, Wiley, Hoboken, 2017, pp. 127–166.
47 X. Wang, Z. Yang, H. Tian, Y. Li, M. Li, W. Zhao, C. Zhang, T. Wang, J. Liu, A. Zhang, D. Shen, C. Zheng, J. Qi, D. Zhao, J. Shi, L. Jin, J. Rao and W. Zhang, *Oncotarget*, 2017, **8**(15), 24892–24901.
48 B. Arévalo, V. Serafín, M. Garranzo-Asensio, R. Barderas, P. Yáñez-Sedeño, S. Campuzano and J. M. Pingarrón, *Biosens. Bioelectron.: X*, 2023, **13**, 100325.
49 S. E. F. Melanson, M. J. Tanasijevic and P. Jarolim, *Circulation*, 2007, **116**, e501–e504.
50 D. V. Grigorieva, I. V. Gorodki, A. V. Sokolov, O. V. Kosmachevskaya, A. F. Topunov, I. V. Buko, E. E. Konstantinova, S. N. Cherenkevich and O. M. Panasenko, *Bull. Exp. Biol. Med.*, 2013, **155**, 118–121.
51 B. Arévalo, M. Blázquez-García, A. Valverde, V. Serafín, A. Montero-Calle, G. Solís-Fernández, R. Barderas, P. Yáñez-Sedeño, S. Campuzano and J. M. Pingarrón, *Bioelectrochemistry*, 2022, **146**, 108157.
52 E. S. Vanamee and D. L. Faustman, *Front. Immunol.*, 2023, **14**, 1225704.
53 J. M. Andrade and M. G. Estévez-Pérez, *Anal. Chim. Acta*, 2014, **838**, 1–12.
54 U. Wallin, B. Glimelius, K. Jirström, S. Darmanis, R. Y. Nong, F. Pontén, C. Johansson, L. Påhlman and H. Birgisson, *Br. J. Cancer*, 2011, **104**, 1619–1627.
55 K. Jakubowska, A. Pryczynicz, V. Dymicka-Piekarska, D. Cepowicz, D. Jagodzińska, Ł. Lewczuk, A. Lebelt, M. Ozimkiewicz, P. Kiszło and K. Guzińska-Ustymowicz, *Prog. Health Sci.*, 2016, **6**(1), 40–48.
56 D. A. Brown, R. L. Ward, P. Buckhaults, T. Liu, K. E. Romans, N. J. Hawkins, A. R. Bauskin, K. W. Kinzler, B. Vogelstein and S. N. Breit, *Clin. Cancer Res.*, 2003, **9**, 2642–2650.
57 R. Barderas, M. Mendes, S. Torres, R. A. Bartolomé, M. López-Lucendog, R. Villar-Vázquez, A. Peláez-García, E. Fuente, F. Bonilla and J. I. Casal, *Mol. Cell. Proteomics*, 2013, **12**, 1602–1620.
58 M. Vocka, D. Langer, V. Fryba, J. Petrtyl, T. Hanus, M. Kalousova, T. Zima and L. Petruzelka, *Cancer Biomarkers*, 2018, **21**(4), 869–874.
59 I. F. Kamel, H. M. Elsadek, A. Mokhtar Ahmad and A. I. Elagrody, *Egypt. J. Hosp. Med.*, 2021, **85**(2), 3639–3644.
60 C. Lungulescu, D. Sur, Ś. Răileanu, Ś. M. Dumitru, E. A. Dumitrescu and C. Virgil Lungulescu, *J. Med. Rad. Onc.*, 2022, **II**(1), 1–8.
61 H. Xue, B. Lü, J. Zhang, M. Wu, Q. Huang, Q. Wu, H. Sheng, D. Wu, J. Hu and M. Lai, *J. Proteome Res.*, 2010, **9**, 545–555.
62 H. Zheng, S. Yu, C. Zhu, T. Guo, F. Liu and Y. Xu, *Exp. Cell Res.*, 2021, **398**, 112394.